



Spectral response of optical fiber probe with closely spaced fibers

Steven L. Jacques

Department of Bioengineering, University of Washington, Seattle, WA, USA

Correspondence to: Steven L. Jacques. Bioengineering, Foegen Bldg. N410G, 3720 15th Ave NE, Box 355061, Seattle, WA 98195-5061, USA. Email: stevjacq@uw.edu.

Background: Optical fiber probe spectroscopy can characterize the blood content, hemoglobin oxygen saturation, water content, and scattering properties of a tissue. A narrow probe using closely spaced fibers can access and characterize a local tissue site, but analysis requires the proper light transport theory.

Methods: Monte Carlo simulations of photon transport specified the response of a two-fiber probe as a function of optical properties in a homogeneous tissue. The simulations used the dimensions of a commercial fiber probe (400-micron-diameter fibers separated by 80-microns of cladding) to calculate the response to a range of 20 absorption and 20 reduced scattering values. The 400 simulations yielded an analysis grid (lookup table) to interpolate the probe response to any given pair of absorption and scattering properties.

Results: The probe in contact with tissue is not sensitive to low absorption but sensitive to scattering, as occurs for red to near-infrared spectra. The probe is sensitive to both absorption and scattering for shorter visible spectra (purple-orange). The non-contact probe held above the tissue delivers light to/from a spot on the tissue and fails to collect light that spreads laterally to escape outside the collection spot. Such partial collection can distort the spectra.

Conclusions: Optical fiber spectroscopy using closely spaced fibers requires proper calibration. An analysis subroutine is provided for analysis of a two-fiber probe with the dimensions of a commercial probe (Ocean Insight), but the method can be applied to any probe design. A closely spaced fiber probe can document blood in the shorter visible wavelengths, but has difficulty detecting red and near-infrared absorption. Hence detection of hydration is difficult. The strength of the closely spaced fiber probe is detecting scattering that depends on tissue structure at the micron to sub-micron scale.

Keywords: Optical fiber; spectroscopy; Monte Carlo

Submitted Jun 30, 2020. Accepted for publication Nov 17, 2020.

doi: 10.21037/qims-20-816

View this article at: <http://dx.doi.org/10.21037/qims-20-816>

Introduction

The ability to assess a tissue's status by a quick low-cost non-invasive optical measurement can find many uses in clinical medicine. Optical spectroscopy can monitor inflammation (1), edema (2), assess metabolic consumption of oxygen (3), detect nuclear abnormalities (4), and quantify fibrosis or stromal remodeling, to mention a few examples. Optical fiber spectrometers are especially convenient for topical placement of a probe to characterize a tissue site, for example on skin (5), oral cavity (1), uro-genital (6), gastrointestinal tract (7), brain (8,9), breast (10), kidney (11),

liver (12), and bronchi (13).

This report considers the use of closely spaced optical fibers in a spectroscopic probe, one fiber for light delivery and one fiber for light collection. The fiber separation is less than 1 mm, which interrogates a local tissue site. Bigio and colleagues pioneered such spectroscopy (14-16), which is especially sensitive to the light scattering properties of a tissue and is called Elastic Scattering Spectroscopy (ESS).

A two-fiber probe on a tissue site delivers light into the tissue with one optical fiber and collects light with the second optical fiber. The lateral separation between the two

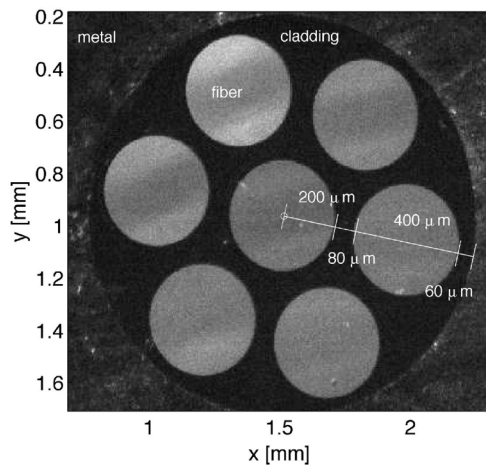


Figure 1 Photograph of the optical fiber probe, where six source fibers surround a central collection fiber. Optical fiber probe, R400-7-UV-VIS, Ocean Insight, Largo, FL, USA; numerical aperture 0.22 ± 0.02 , equivalent to an acceptance angle of 24.8° in air.

optical fibers as they contact the tissue determines the tissue depth that the measurement interrogates. Larger separation yields a deeper measurement. Closer separation yields a more superficial measurement. The interaction of the probe response with the inter-fiber separation and the wavelength-dependent tissue optical properties are quite non-linear (17). Therefore, light transport theory is used to understand the interaction and to interpret measurements.

Diffusion theory provides a simple light transport calculation that usually works well when the fiber separation is greater than 1 or 2 mm. Often one wishes a more compact probe where the optical fiber separation is much closer. One may wish a more superficial measurement, or one may not have much room for a wide probe with large fiber separations. Diffusion theory fails for such closely spaced fibers.

This report analyzes the generic case of a two-fiber probe spaced less than 1 mm apart. In particular, a widely used commercially available optical fiber probe is considered, which arranges six source fibers around a central collection fiber, where the 400- μm -core-dia. optical fibers are separated by 80 μm (480 μm center-to-center). Its behavior is the same as the generic two-fiber probe. The particular commercial probe design of this report was chosen due to its wide use and reproducible construction, however, the method described in this report can be applied to all such probes. This report will be useful for investigators using spectroscopy for clinical, biomedical, or industrial

measurements.

The report considers the probe response when the probe is in contact with a tissue but with near-zero pressure to avoid disturbing the blood perfusion, which is the situation when a local region of a tissue site is being interrogated by a lightly placed probe. Secondly, the non-contact probe response is considered, where the probe is held above the tissue surface yielding a generic diffuse reflectance measurement that is no longer sensitive to the particular inter-fiber spacing of the probe. The results show that the contact probe is not sensitive to the absorption of low-absorption tissues, but sensitive to high absorption and to the scattering properties. The non-contact probe is sensitive to both absorption and scattering, and delivers and collects light from the same spot on the tissue. Therefore lateral diffusion of light allows some light to escape outside this spot and hence escape collection. Such partial collection of light can distort the measured spectra.

A commercial optical fiber probe

Figure 1 shows the face of a commercial multi-fiber probe (400- μm fiber probe, Ocean Insight, Largo, FL, USA) with six source fibers surrounding a single central collection fiber. Monte Carlo simulations were conducted to calculate the delivery and collection of light by the probe. In this report, two conditions were tested: (I) a contact probe, where the probe was assumed to be placed in contact with a tissue, and (II) a non-contact probe, where the probe was held 1 cm above the tissue. The model assumed a homogeneous tissue with uniform absorption and reduced scattering properties. However, the Monte Carlo simulation can be adjusted to model complex tissues, such as a multi-layered tissue like epidermis/dermis or epithelium/stroma. The method reported here can be applied to those simulations. Alternative probe designs with different fiber positions and separations can also be simulated and the method applied.

Methods

Probe in contact with tissue

Monte Carlo simulations of the probe in contact with tissue were conducted. The simulations used mcml.c (18), a cylindrically symmetrical calculation of light transport, to generate point spread functions of escaping flux density at the tissue/probe interface, labeled $R(r)$ (W/cm^2 escaping per W delivered) or (cm^2), where r denotes the separation

Table 1 Typical soft tissue parameters that govern tissue optical properties. Three values for blood content (B) are given

Parameter	Symbol	Value
Blood content	B	0.001, 0.01, 0.05
Hemoglobin oxygen saturation	S	0.75
Water content	W	0.65
Scattering strength, $\mu_s'(500\text{ nm})$	a	15 cm^{-1}
Scattering power	b	1

between a point source and the position of escape. A range of optical properties were used in 400 simulations: 20 absorption coefficients, μ_a , logarithmically distributed from 0.01 to 100 (cm^{-1}), and 20 reduced scattering coefficients, $\mu_s' = \mu_s(1-g)$, logarithmically distributed from 1 to 300 (cm^{-1}). μ_s is the scattering coefficient and g is the anisotropy equal to the mean value of $\cos(\theta)$ where θ is the photon deflection angle of a single scattering event, typically $g \approx 0.90$. These ranges are broader than normally found in tissues in order to illustrate the generic behavior of this probe design.

The simulations considered the transport of light from a single source fiber to a single collection fiber. For each μ_a, μ_s' pair, the point spread function specified by the simulation was convolved over the face of the source fiber and the light collected over the face of the collection fiber was summed. The result was a single value of collection in units of (W collected/W delivered) or (dimensionless) for a μ_a, μ_s' pair. Because the collected power was normalized by the delivered power, the result for a single two-fiber probe was the same as for a 6-surrounding-1 fiber probe for a homogeneous tissue. Repeating this convolution for all 400 μ_a, μ_s' pairs yielded an analysis grid (i.e., a look-up table) of $R_{\text{probe}}(\mu_a, \mu_s')$ (W collected per W delivered) or (dimensionless).

The expected values of μ_a, μ_s' values for a typical soft tissue from 300 to 1,000 nm wavelength was specified by the parameters in *Table 1* for the case of a 1% blood content using the following expressions for each wavelength λ :

$$\begin{aligned} \mu_a(\lambda) &= BS\mu_{a,\text{oxy}}(\lambda) + B(1-S)\mu_{a,\text{deoxy}}(\lambda) + W\mu_{a,\text{water}}(\lambda) \\ \mu_s'(\lambda) &= a(\lambda / 500\text{ nm})^{-b} \end{aligned} \quad [1]$$

where $\mu_{a,\text{oxy}}$, $\mu_{a,\text{deoxy}}$, and $\mu_{a,\text{water}}$ are the absorption spectra of oxygenated hemoglobin, deoxygenated hemoglobin, and water, respectively, from the website <https://omlc.org/spectra/>. The factor a is the scattering strength [$a =$

$\mu_s'(500\text{ nm})$], and b is the scattering power. *Table 1* lists the other parameters.

Figure 2A shows the point spread functions calculated by Monte Carlo simulations for escaping flux density as a function of radial position, $R(r)$ (cm^{-2}). Each $R(r)$ curve is for a different pair of absorption (μ_a) and scattering (μ_s') coefficients. The figure shows the location of the source and collection fibers.

Figure 2B shows a histogram of all distances between source fiber pixels and collection fiber pixels on the faces of the two fibers, based on a 400- μm -dia. fibers. The mean distance is 408 μm .

Figure 2C shows the analysis grid $R_{\text{probe}}(\mu_a, \mu_s')$ (dimensionless) based on the Monte Carlo simulations. There is an interval of scattering (x-axis μ_s') around $10^{1.56} = 36\text{ cm}^{-1}$ in which the strongest probe response occurs. If scattering is too low, the light spreads out in the tissue beyond the collection fibers, so the collected signal drops. If the scattering is too high, the delivered light is prevented from reaching the collection fiber, so again the signal drops. But when the scattering is around 36 cm^{-1} , the scattering is optimal for restricting the light within the tissue around the collection fiber and the collection fibers see a maximum density of escaping flux.

As the absorption initially increases (y-axis μ_a), there is initially little change in R_{probe} because the absorption is so low. The photons scatter to the collector through short pathlengths dominated by the scattering coefficient, so the pathlength [L (cm)] spent by collected photons in the tissue is short. Hence, the attenuation of light, $\exp(-\mu_a L)$, is small because photon pathlength L is small. When the absorption becomes stronger ($\mu_a > 1\text{ cm}^{-1}$), the probe become more strongly responsive to the tissue's absorption. In other words, when in contact with a low-absorption tissue, the probe is primarily responsive to the tissue's scattering properties, which depend on the micron and sub-micron scale of tissue structure. This behavior is due to the close spacing of source and collection fibers. There is always some effect of absorption on the signal due to the background diffuse reflectance involving deeper tissue, but this diffuse signal has spread out beyond the collection fibers and hence is largely not collected.

Figure 2C includes the locus of the μ_a, μ_s' pairs calculated {see Eq. [1]} for a generic tissue with the parameters in *Table 1* for the case of a 1% blood content. In other words, this is the reflectance spectrum of the tissue.

Figure 2D shows the analysis grid $R_{\text{probe}}(\mu_a, \mu_s')$ based on diffusion theory (18). The general pattern of this grid is

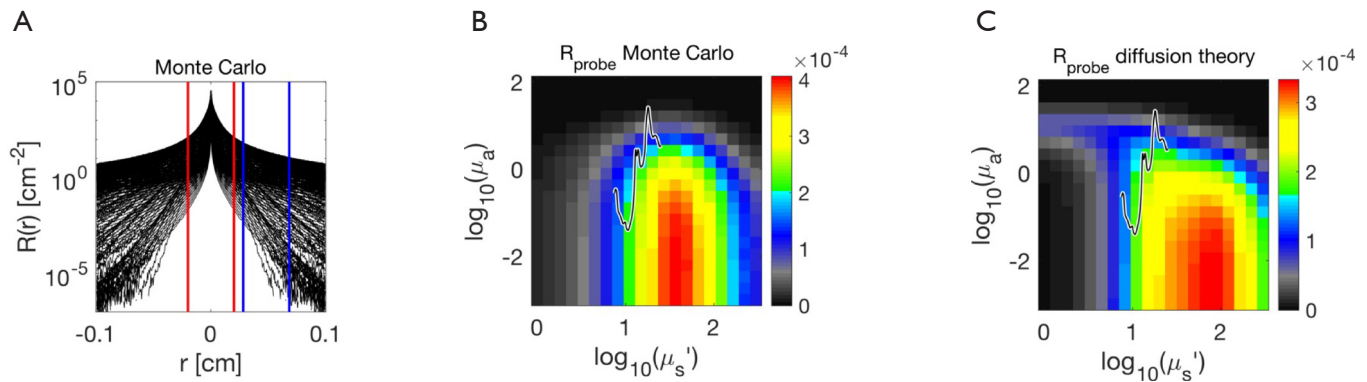


Figure 2 (A) Point spread functions (PSFs) for escaping flux as a function of radial position r [reflectance $R(r)$ (cm^{-2})]. The size and location of one source fiber and the central collection fiber are indicated. Each $R(r)$ curve is for a different pair of absorption (μ_a) and scattering (μ_s') coefficients. (B) Histogram of the distances between source fiber pixels and collection fiber pixels. The average distance is $408 \mu\text{m}$. (C) After convolution of the PSFs over the $400\text{-}\mu\text{m}$ -dia. source fiber, the probe response is shown as an analysis grid $R_{\text{probe}}(\mu_a, \mu_s')$ ($W_{\text{collected}}/W_{\text{delivered}}$) or (dimensionless) based on the Monte Carlo simulations. The black/white line is the locus of μ_a, μ_s' pairs in the absorption and scattering spectr for a typical tissue with blood content =1%, oxygen saturation of hemoglobin =75%, water content =65%, $\mu_s' = (15 \text{ cm}^{-1}) (\lambda/500 \text{ nm})^{-1}$, $\lambda = 300\text{--}1,000 \text{ nm}$ wavelength. (D) The analysis grid $R_{\text{probe}}(\mu_a, \mu_s')$ based on diffusion theory (18).

similar to the grid generated by Monte Carlo simulations, but there are clear differences that occur in the range of μ_a, μ_s' values typical for tissues. The differences become greater for high absorption and low scattering, which diffusion theory does not adequately model.

The Supplement presents a subroutine $R_{\text{probe}}(\mu_a, \mu_s') = \text{getRprobe}(\mu_a, \mu_s')$ that is based on 2D-interpolation of the analysis grid of *Figure 2C* (Appendix 1).

Figure 3 shows the iso- μ_s' curves of R_{probe} for the range of μ_a values, and the iso- μ_a curves of R_{probe} for the range of μ_s' values. The curves show rather slow gradients of change as properties change, which reassures that the 2D interpolation used in $\text{getRprobe}(\mu_a, \mu_s')$ will behave well.

Probe not in contact with tissue

A second analysis grid was also prepared for the probe not in contact with a tissue (*Figure 4*). The probe was held above the tissue at a height of 1.0 cm and delivered light as a conical beam between $\pm 24.8^\circ$. The irradiance was assumed to be uniform over the illuminated spot for this example. A Gaussian-shaped intensity of illumination from the probe source fibers would alter the response a little, because the irradiance would be non-uniform. The flux escaping across the air/tissue boundary (a refractive index mismatch $n_{\text{tissue}}/n_{\text{air}} = 1.4$) was recorded for each μ_a, μ_s' pair as local diffuse reflectance $R(r)$ (cm^{-2}), and as total diffuse reflectance, R_d

(dimensionless).

The six source fibers create six spots of illumination, which closely overlap since the inter-fiber spacing is so small compared to the size of the illuminated spots. The central collection fiber collects reflectance from essentially the same spot to which light is delivered. Lateral spread in the tissue causes some of the escaping flux to not be collected. Hence, the probe measures a lower value than the true total diffuse reflectance, R_d . There is also a component of specular reflectance from the tissue surface that is collected by the probe, which does not contain information about the tissue properties.

The following subsection first considers the total diffuse reflectance (R_d) as a function of the optical properties μ_a, μ_s' . The second subsection considers the effect of partial collection (f_{esc}) where the probe does not collect the peripheral ring of light that has spread outside the collection spot of the probe.

Total $R_d(\mu_a, \mu_s')$

Figure 5A shows the analysis grid $R_d(\mu_a, \mu_s')$ based on Monte Carlo simulations. As scattering increases, the R_d increases. As absorption increases, R_d decreases. The black line shows the $R_d(\lambda)$ spectrum expected for a tissue with the properties in *Table 1* for the case of 1% blood volume. The spectrum extends from $300\text{--}1,000 \text{ nm}$.

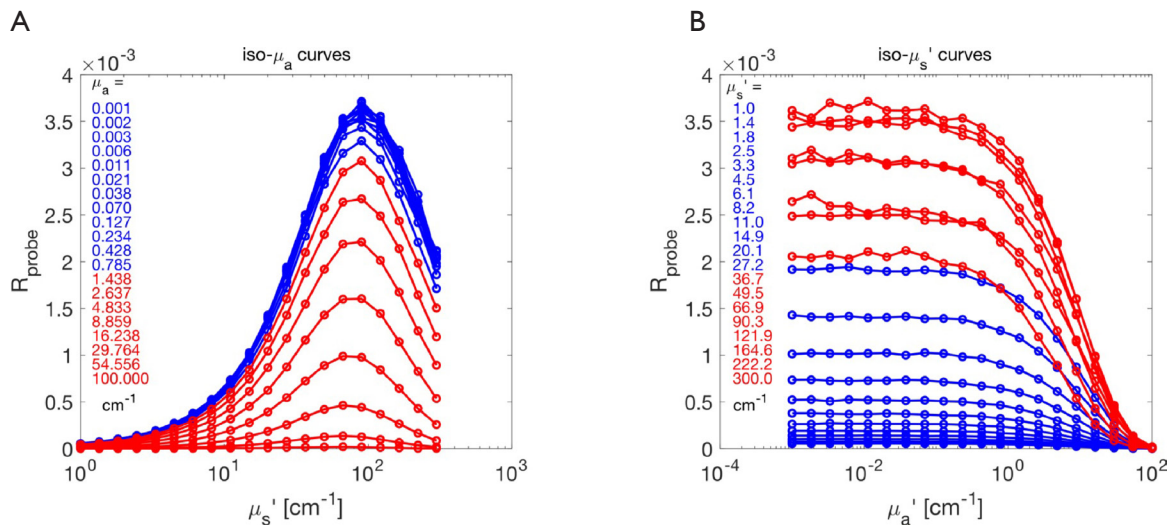


Figure 3 (A) Iso- μ_a curves of R_{probe} for the range of μ_a values. (B) Iso- μ_s' curves of R_{probe} for the range of μ_s' values.

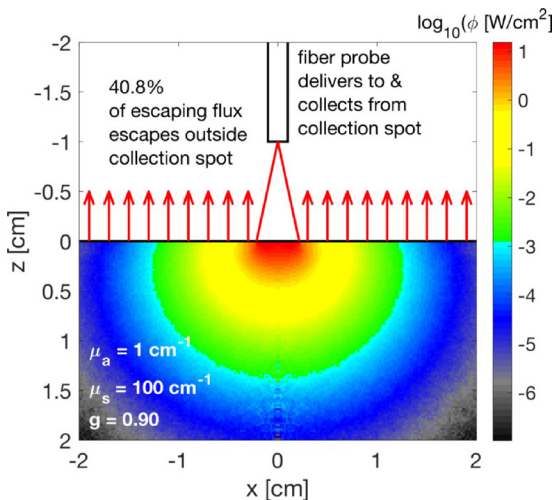


Figure 4 The optical fiber probe delivers light to and collects light from a collection spot, $r \leq h \tan(\theta)$, where h is the fiber height above the tissue. In this example, $h = 1$ cm and 59.2% of the light escapes within the collection spot, while 40.8% escapes outside the spot. The probe then only collects $f_{coll} = 2 \times 10^{-4}$ of this light escaping within the collection spot [see Eq. [1]] In this example, $R_d = 0.260$. The net collection is $0.260 \times 0.592 \times 2 \times 10^{-4} = 3.1 \times 10^{-5}$.

Partial collection of $R_d(\mu_a, \mu_s')$ by non-contact probe

Figure 4 showed the delivery and collection of light by the optical fiber probe to/from a circular spot [radius $\leq h \tan(\theta)$, where fiber height $h = 1$ cm]. The simulation was adjusted to deliver an expanding beam of light that illuminated this spot

uniformly, which is a simplification to illustrate the effect of partial collection by the cone of light delivered and collected by the probe. The maximum half-angle of delivery/collection was $\theta = 24.8^\circ$, which depends on the numerical aperture of the optical fiber. Within the tissue the light spreads and only a fraction (f_{esc}) of the total escaping light (R_d) escapes within this collection spot. A fraction $(1 - f_{esc})R_d$ escapes outside the collection spot. In this example ($\mu_a = 1$ cm $^{-1}$, $\mu_s' = 100$ cm $^{-1}$, $g = 0.90$), only 59.2% of the escaping flux escapes within the collection spot ($f_{esc} = 0.592$). Then only a fraction of this light, $f_{coll} \approx (\pi a^2)/(2\pi h^2)$, is collected by the collection fiber of the probe (radius $a = 200$ μm). Therefore, the fraction of total reflectance (R_d) that is collected by the probe is f ,

$$\begin{aligned}
 f_{esc} &= R(r \leq h \sin(\theta)) / R_d \\
 f_{coll} &= (\pi a^2) / (2\pi h^2) \\
 f &= f_{esc} f_{coll}
 \end{aligned}
 \tag{2}$$

where $f_{esc} = 0.592$, $f_{coll} = 2 \times 10^{-4}$, and $f = 1.19 \times 10^{-4}$ in the example of Figure 4. The factor f_{esc} depends on the tissue optical properties and the spot size of collection.

Figure 5B shows $f_{esc}(\mu_a, \mu_s')$, illustrating how f_{esc} drops when absorption or scattering become too low and light spreads laterally outside the collection spot. For high absorption or scattering, most of the escaping photons escape within the measurement spot and f_{esc} approaches 1.0.

Figure 5C shows the analysis grid for the product $R_d f_{esc}$, which is the response for the probe held 1 cm above a tissue.

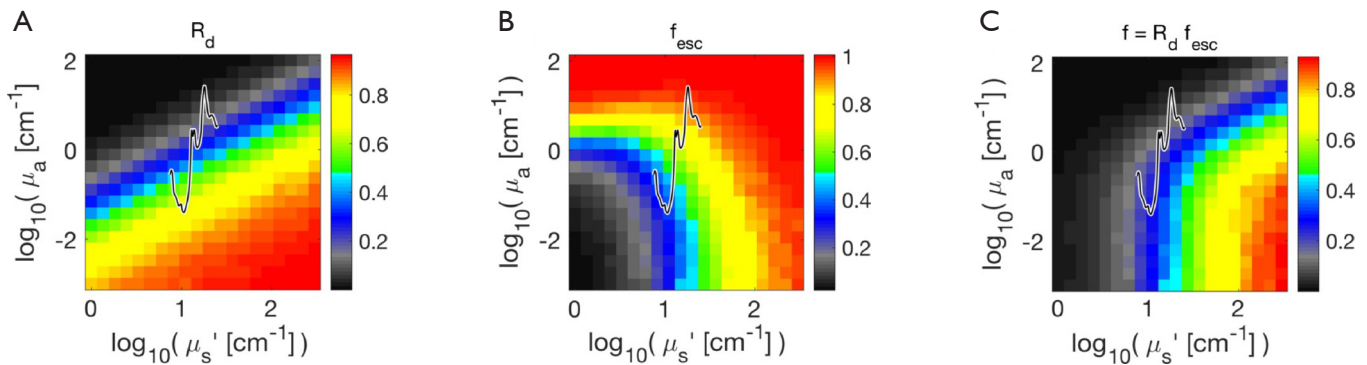


Figure 5 Analysis grids for non-contact probe. (A) Total diffuse reflectance, $R_d(\mu_a, \mu_s')$, based on Monte Carlo simulations. Diffusion theory yields nearly the same grid (not shown). (B) The collection fraction $f_{\text{esc}}(\mu_a, \mu_s')$. (C) The product $R_d f_{\text{esc}}$, which shows the distortion due to partial collection of light from only the collection spot for the probe 1 cm above the tissue. The black line shows the locus of μ_a, μ_s' pairs expected for the absorption and scattering spectra of the generic tissue in *Table 1* with 1% blood.

Comparing with *Figure 5A*, there is significant distortion of the non-contact probe response due to photons at wavelengths of low absorption and low scattering escaping outside the collection spot of the probe.

Results

Using analysis grid to predict probe response: the forward problem

Once the analysis grid has been prepared, it may be used to predict the R_{probe} spectrum given particular tissue parameters that determine the optical properties of the tissue over a range of wavelengths. This is called the “forward problem” in which known tissue parameters are used to predict an observed R_{probe} spectrum. Given a μ_a, μ_s' pair at each wavelength, the subroutine `getRprobe(μ_a, μ_s')` yields the expected R_{probe} spectrum. This subroutine is listed in the Supplement and is based on the Monte Carlo simulation of the response for the probe in *Figure 1* (Appendix 1).

Figure 6 shows the three spectra generated by the μ_a, μ_s' pairs generated by Eq. [2] for each wavelength based on the tissue parameters in *Table 1*. The spectra are generated by 2D-interpolation of $\log_{10}(\mu_a), \log_{10}(\mu_s')$ against the analysis grid. *Figure 6A* shows the spectra expected when the probe is held in contact with tissue using the $R_{\text{probe}}(\mu_a, \mu_s')$ analysis grid.

Figure 6B shows the spectra expected when the probe is held 1 cm above the tissue using the $R_d(\mu_a, \mu_s')$ analysis grid (see `getRd()` in Appendix 1). The total R_d spectra are shown as black lines. The $R_d f_{\text{esc}}$ spectra (red lines) show the

reflectance escaping within the collection spot of the fiber probe. The $R_d f_{\text{esc}}$ spectra are distorted due to the loss of collected reflectance at wavelengths with low absorption and low scattering because light spreads within the tissue and escapes outside the collection spot. The final term f_{coll} is ignored in this figure, since it simply scales the spectra by 2×10^{-4} but does not distort the spectra.

Note that the non-contact $R_d(\lambda)$ spectra (black lines) show more sensitivity to absorption at long wavelengths than do the contact $R_{\text{probe}}(\lambda)$ spectra for the probe in contact with the tissue. The contact probe collects photons that have spent a short pathlength in the tissue, and hence low absorption does not have a chance to exert an effect. In particular, note how the absorption by water in the tissue is seen as a dip in R_d at 960 nm, but is not significant in R_{probe} . Also, the slight dip at 760 nm due to deoxy-hemoglobin is seen in R_d but not in R_{probe} . However, the $R_d f_{\text{esc}}$ spectra (red lines) have lost much of this advantage of sensitivity to low absorption since long-pathlength photons are lost.

Therefore, it is better to deliver light via other fibers (or light sources) illuminating an area much broader than the collection spot so that the problem of partial collection is avoided. Then the collection by the central fiber of the probe will not suffer distortion at wavelengths of low absorption and low scattering. The probe will sample the total reflectance without distortion.

Using analysis grid to analyze probe response: the inverse problem

The “inverse problem” strives to deduce the tissue

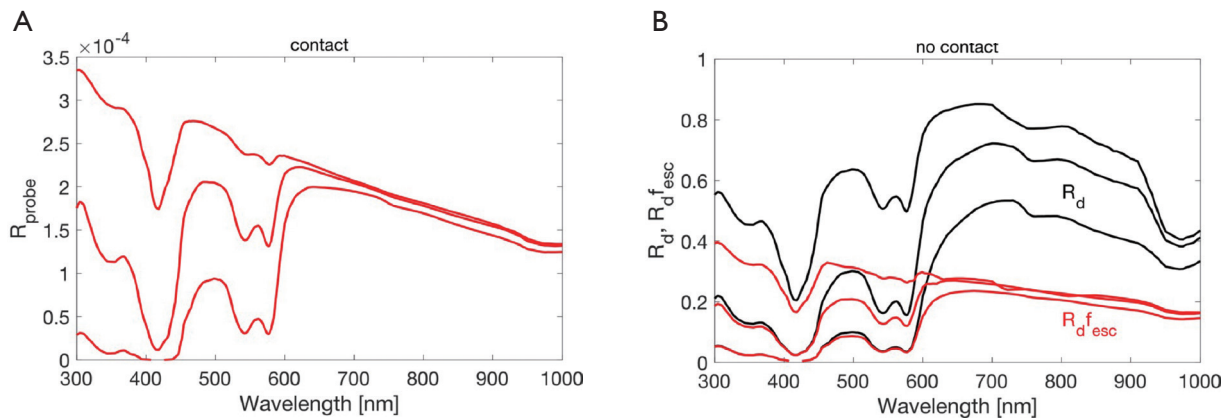


Figure 6 The reflectance spectra predicted by interpolating the analysis grids for the μ_a, μ_s' pairs generated by Eq. [1] for each wavelength based on the tissue parameters in *Table 1*. (A) Using $R_{probe}(\mu_a, \mu_s')$ as the analysis grid (probe in contact with tissue). (B) Using $R_d(\mu_a, \mu_s')$ as the analysis grid (non-contact probe 1 cm held above tissue). The R_d spectra (black lines) equal the total diffuse reflectance. The $R_d f_{esc}$ spectra (red lines) show the reflectance escaping from the collection spot, illustrating the distortion of spectra due to the partial collection by the non-contact probe. The final term f_{coll} is ignored here, since it simply scales the spectra by 2×10^{-4} and does not distort the spectra.

parameters (*Table 1*) based on the measured contact-probe spectra M_{probe} or the non-contact total reflectance measurement M_d , where M indicates the uncalibrated measurement in units of (counts). In this section, M_{tissue} and R_{tissue} refer to either M_{probe} and $getRprobe()$ or M_d and $getRd()$, depending on whether a contact or non-contact probe is being used. The protocol is listed in two steps:

Take ratio of tissue spectrum to reference spectrum

A reference spectral measurement $M_{std}(\lambda)$ is made by placing the probe above a calibrated reflectance standard, e.g., a SpectralonTM reflectance standard ($R_{std}=0.99$; Labsphere Inc., NH, USA). It is important that the $M_{std}(\lambda)$ is acquired while the probe is not in contact with the reference standard. Otherwise, both the $\mu_a(\lambda)$ and $\mu_s'(\lambda)$ of the standard must be known in order to calibrate. A non-contact measurement needs to know only the calibrated $R_{std}(\lambda)$ of the standard reference, which is usually supplied by the manufacturer. The normalized measurement M (dimensionless) for each wavelength is,

$$M = M_{tissue} / M_{std} = (R_{tissue} f_{tissue}) / (R_{std} f_{std}) = K R_{tissue} / R_{std} \quad [3]$$

where $K = f_{tissue} / f_{std}$. The factor f is the collection efficiency of the measurement on the tissue or reference standard. The geometry of the tissue measurement and the reference measurement need not be the same. For example, a contact measurement has an f_{tissue} that depends on the solid angle of collection by the fiber (Ω) and the

fiber collection area (A_{fiber}): $f_{tissue} \approx (\Omega/2\pi)A_{fiber}$. The f_{std} for the reference measurement from some height (h) above the reflectance standard depends on h and A_{fiber} : $f_{std} \approx A_{fiber} / (2\pi h^2)$. The tissue measurement may be from a different height than the standard measurement. The factor K is usually an unknown experimental parameter, however it is nearly wavelength-independent and hence scales but does not affect the shape of the spectrum. Eq. [3] is rearranged to place measurements on the left and the least-squares fit on the right,

$$R_{std} M_{tissue} / M_{std} = K R_{tissue} \quad [4]$$

Least-squares fitting solves for tissue parameters

Least-squares fitting is applied to match the left and right sides of Eq. [4] to determine $B, S, a, b,$ and K , where a is the scattering strength [$a = \mu_s'(\lambda_{ref})$, e.g., $\lambda_{ref} = 500$ nm] and b is the scattering power. The water content W is assigned an assumed value (e.g., $W = 0.50$). The B, S, a, b are used in Eq. [1] to specify $R_{tissue}(\lambda)$, and K scales the result. The fitting strives to match the shape of the spectrum, not the absolute value, since the shape is scaled by K .

To illustrate, *Figure 7* shows the fitting of two skin spectra taken by (A) the probe in contact with skin, and (B) the non-contact probe. An additional attenuation, $\exp(-m \mu_{a,melanin} L_{epidermis})$, is included in the analysis to account for the slight amount of melanin in these skin Type II sites (m = melanosome volume fraction in a 60- μ m-thick epidermis,

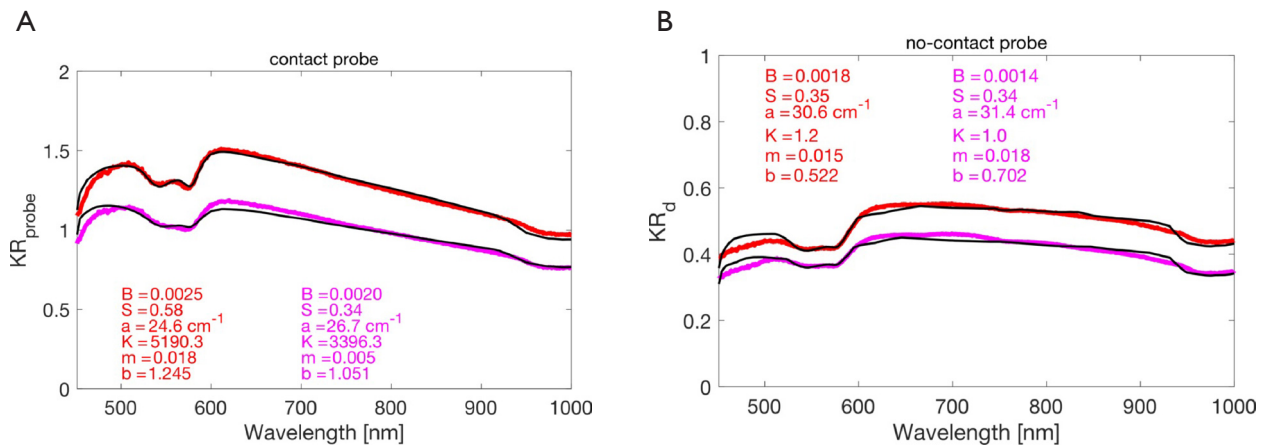


Figure 7 Two skin spectra. (A) Spectrum acquired by the probe in contact with lightly pigment forearms. Black lines are the least-squares fit using `getRprobe()`, which is for a homogeneous tissue and hence not optimized for skin. The water content is set to 0.50. (B) Spectrum acquired by non-contact probe.

$L_{\text{epidermis}}$ is the pathlength spent in the epidermis by escaping photons, which is about three times the epidermal thickness or 180 μm , based on Monte Carlo simulations of skin as increments of melanin are added to the epidermis). The values of B , S , a , b , m and K are shown in *Figure 7*. This analysis assumes a homogeneous skin with a superficial absorbing filter due to epidermal melanin, and therefore is not as accurate as a multi-layered Monte Carlo simulation of the skin.

The contact probe shows higher blood content than the non-contact probe, likely due to interrogating the superficial vascular plexus while the non-contact probe also interrogates the reticular dermis with a lower blood content. The contact probe shows a slightly lower scattering strength (a) with a higher scattering power (b), perhaps indicating the difference between scattering in the papillary dermis versus the reticular dermis. The papillary dermis may have smaller collagen fiber bundles than the reticular dermis yielding a smaller scattering strength. The higher b implies a shift toward smaller scale scattering as if the smaller collagen fibrils are not as tightly cross-linked into fiber bundles and are able to behave more like Rayleigh scatterers whose scattering falls more rapidly with wavelength. These conjectures are cited only to suggest how future work could learn about tissue structure from such contact and non-contact probe spectra.

Discussion

This paper is a technical report important for users

of optical spectroscopic technology to understand the strengths and weaknesses of a very common type of optical fiber probe that uses two closely spaced fibers. The six-surrounding-one fiber probe in this report will behave the same as a two-fiber probe with one source and one collector, with respect to the variation in signal versus optical properties, although the magnitude of the signal will differ.

The Monte Carlo model in this paper assumed a tissue with homogeneous optical properties. Obviously, this assumption breaks down for complex tissue architectures, such as skin with its multiple layers. However, the model does fit experimental data when the probe is in contact with skin and provides a practical metric for following changes in blood content (B), oxygen saturation (S). For unpigmented tissues, the probe and model can follow changes in B and S . For skin with epidermal melanin, a superficial melanin filter can be included to attenuate the prediction of the homogeneous model (19). The behavior of the probe when held above the skin (non-contact measurement) is illustrated in *Figure 7*, which cautions about the partial collection of total reflectance that may distort a spectrum.

Conclusions

When an optical fiber probe with closely spaced fibers contacts a tissue (or medium), the response is not sensitive to low absorption values, but is sensitive to μ_a values above 1 cm^{-1} . The contact probe is sensitive to the scattering properties of the tissue. Therefore, such probes can follow

inflammation using the shorter wavelength range and follow structural changes using the longer wavelength range.

When the probe is held above a tissue as a non-contact measurement, the total diffuse reflectance spectrum, $R_d(\lambda)$, is expected to be sensitive to both absorption and scattering. However, the probe only collects from the spot of illumination, which is specified by the numerical aperture of the fibers and the height of the fiber above the tissue. Consequently, many photons at wavelengths of low absorption and low scattering escape the tissue outside this collection spot, as described by $f_{esc}(\mu_a, \mu_s)$. The probe collects $R_d f_{esc}$. Therefore, the non-contact probe loses some of the advantage of R_d for low-absorption sensitivity. If light is delivered more broadly by separate illumination so the non-contact probe samples the central region of a larger illuminated area, then the non-contact measurement will avoid wavelength-dependent losses that distort the spectrum.

Acknowledgments

Funding: None.

Footnote

Provenance and Peer Review: With the arrangement by the Guest Editors and the editorial office, this article has been reviewed by external peers.

Conflicts of Interest: The author has completed the ICMJE uniform disclosure form (available at <http://dx.doi.org/10.21037/qims-20-816>). The special issue “Advanced Optical Imaging in Biomedicine” was commissioned by the editorial office without any funding or sponsorship. The author has no other conflicts of interest to declare.

Ethical Statement: This paper did not involve a clinical study. The arm spectra of *Figure 7* were spectra acquired several years ago at Tufts University under an approved protocol (Prof. Sergio Fantini).

Open Access Statement: This is an Open Access article distributed in accordance with the Creative Commons Attribution-NonCommercial-NoDerivs 4.0 International License (CC BY-NC-ND 4.0), which permits the non-commercial replication and distribution of the article with the strict proviso that no changes or edits are made and the original work is properly cited (including links to both the

formal publication through the relevant DOI and the license). See: <https://creativecommons.org/licenses/by-nc-nd/4.0/>.

References

1. Liu KZ, Xiang XM, Man A, Sowa MG, Cholakis A, Ghiabi E, Singer DL, Scott DA. In vivo determination of multiple indices of periodontal inflammation by optical spectroscopy. *J Periodontol Res* 2009;44:117-24.
2. Gill AS, Rajneesh KF, Owen CM, Yeh J, Hsu M, Binder DK. Early optical detection of cerebral edema in vivo. *J Neurosurg* 2011;114:470-7.
3. Liasi FT, Samatham R, Jacques SL. Noninvasive in vivo optical characterization of blood flow and oxygen consumption in the superficial plexus of skin. *J Biomed Opt* 2017;22:1-6.
4. Backman V, Wallace MB, Perelman LT, Arendt JT, Gurjar R, Müller MG, Zhang Q, Zonios G, Kline E, McGilligan JA, Shapshay S, Valdez T, Badizadegan K, Crawford JM, Fitzmaurice M, Kabani S, Levin HS, Seiler M, Dasari RR, Itzkan I, Van Dam J, Feld MS. Detection of preinvasive cancer cells. *Nature* 2000;406:35-6.
5. McKenna J, Pabbies A, Friesen JR, Sowa MG, Hayakawa T, Kerr PD. Assessing flap perfusion: optical spectroscopy versus venous doppler ultrasonography. *J Otolaryngol Head Neck Surg* 2009;38:587-94.
6. Farage MA, Cambron T, Liu KZ. Visible-Near Infrared Spectroscopic Assessment of Urogenital Tissue in Premenopausal and Postmenopausal Women. *Clin Med Insights Womens Health* 2018;11:1179562X17749608.
7. Dhar A, Johnson KS, Novelli MR, Bown SG, Bigio IJ, Lovat LB, Bloom SL. Elastic scattering spectroscopy for the diagnosis of colonic lesions: initial results of a novel optical biopsy technique. *Gastrointest Endosc* 2006;63:257-61.
8. Lin WC, Toms SA, Johnson M, Jansen ED, Mahadevan-Jansen A. In vivo brain tumor demarcation using optical spectroscopy. *Photochem Photobiol* 2001;73:396-402.
9. Villringer A, Chance B. Non-invasive optical spectroscopy and imaging of human brain function. *Trends Neurosci* 1997;20:435-42.
10. Shah N, Cerussi AE, Jakubowski D, Hsiang D, Butler J, Tromberg BJ. The role of diffuse optical spectroscopy in the clinical management of breast cancer. *Dis Markers* 2003-2004;19:95-105.
11. Bensalah K, Peswani D, Tuncel A, Raman JD, Zeltser I, Liu H, Cadeddu J. Optical reflectance spectroscopy to differentiate benign from malignant renal tumors at

- surgery. *Urology* 2009;73:178-81.
12. Nilsson JH, Reistad N, Brange H, Öberg CF, Stuesson C. Diffuse Reflectance Spectroscopy for Surface Measurement of Liver Pathology. *Eur Surg Res* 2017;58:40-50.
 13. Aerts JG, Amelink A, van der Leest C, Hegmans JP, Hemmes A, den Hamer B, Sterenborg HC, Hoogsteden HC, Lambrecht BN. HIF1a expression in bronchial biopsies correlates with tumor microvascular saturation determined using optical spectroscopy. *Lung Cancer* 2007;57:317-21.
 14. Mourant JR, Bigio IJ, Boyer J, Conn RL, Johnson T, Shimada T. Spectroscopic diagnosis of bladder cancer with elastic light scattering. *Lasers Surg Med* 1995;17:350-7.
 15. Bigio IJ, Mourant JR. Ultraviolet and visible spectroscopies for tissue diagnostics: fluorescence spectroscopy and elastic-scattering spectroscopy. *Phys Med Biol* 1997;42:803-14.
 16. Rodriguez-Diaz E, Castanon DA, Singh SK, Bigio IJ. Spectral classifier design with ensemble classifiers and misclassification-rejection: application to elastic-scattering spectroscopy for detection of colonic neoplasia. *J Biomed Opt* 2011;16:067009.
 17. Wang L, Jacques SL, Zheng L. MCML--Monte Carlo modeling of light transport in multi-layered tissues. *Comput Methods Programs Biomed* 1995;47:131-46.
 18. Farrell TJ, Patterson MS, Wilson B. A diffusion theory model of spatially resolved, steady-state diffuse reflectance for the noninvasive determination of tissue optical properties in vivo. *Med Phys* 1992;19:879-88.
 19. Jacques SL, Samatham R, Choudhury N. Rapid spectral analysis for spectral imaging. *Biomed Opt Express* 2010;1:157-64.

Cite this article as: Jacques SL. Spectral response of optical fiber probe with closely spaced fibers. *Quant Imaging Med Surg* 2021;11(3):1023-1032. doi: 10.21037/qims-20-816

The two subroutines, getRprobe() for the contact probe and getRdprobe() for the non-contact probe, are presented. First, the optical properties of absorption coefficient (m_a [cm^{-1}] labeled ma) and reduced scattering coefficient (m_s [cm^{-1}] labeled msp) used in the Monte Carlo simulations are prepared as follows (MATLAB notation):

```

ma = [
    0.0010    0.0018    0.0034    0.0062    0.0113    0.0207...
    0.0379    0.0695    0.1274,   0.2336    0.4281    0.7848...
    1.4384    2.6367    4.8329    8.8587    16.2378    29.7635,...
    54.5559   100.0];
lma = log10(ma);
msp = [
    1.0000    1.3501    1.8228    2.4611    3.3228    4.4862...
    6.0569    8.1776    11.0407,  14.9064    20.1256    27.1721...
    36.6858   49.5305    66.8725    90.2863    121.8981   164.5780,...
    222.2012  300.0];
lmsp = log10(msp);
[LMSP LMA] = meshgrid(log(msp),log(ma));
for use by the subroutines listed in the following subsections.

```

Contact probe getRprobe()

The subroutine getRprobe() returns the predicted probe response $R_{\text{probe}}(m_a, m_s')$ for a particular m_a, m_s' pair when the probe is in contact with a homogeneous tissue. The subroutine uses 2D interpolation (the function griddata.m in MATLAB):

```

function Rprobe = getRprobe(mu_a,mu_s',LMSP,LMA,gridRprobe)
lmua = log10(mu_a);
lmusp = log10(mu_s');
Rprobe = griddata(LMSP,LMA,Rprobe,lmusp,lmua);
which uses the following array gridRprobe(1:20,1:20) that holds the values for  $R_{\text{probe}}(m_a, m_s')$  [W collected per W delivered]
or [dimensionless]:

```

```

gridRprobe(1:20,1:10) x105 =
    1.5119    2.1049    2.9215    4.1072    5.7454    8.0885    11.3420    15.7080    21.2349    27.6629
    1.5114    2.1030    2.9193    4.0845    5.7741    8.1265    11.3551    15.7185    21.1913    27.6308
    1.5065    2.1088    2.9460    4.1066    5.7494    8.1103    11.3478    15.7192    21.2165    27.4928
    1.5117    2.0939    2.9228    4.1079    5.7561    8.1001    11.3526    15.6246    21.2550    27.5498
    1.5073    2.0819    2.9090    4.0884    5.7241    8.0705    11.2920    15.6186    21.2401    27.4160
    1.5009    2.0902    2.8949    4.0760    5.7509    8.0493    11.2993    15.5453    21.0629    27.2559
    1.4989    2.0687    2.8836    4.0430    5.6565    8.0098    11.1608    15.5100    20.9994    27.2027
    1.4758    2.0366    2.8635    3.9879    5.5860    7.9295    11.0619    15.1843    20.7220    27.0838
    1.4469    2.0011    2.7760    3.9038    5.4832    7.7322    10.8192    15.0323    20.4200    26.5067
    1.3904    1.9233    2.6729    3.7482    5.2617    7.4185    10.4250    14.5963    19.6501    25.5817
    1.3039    1.8025    2.5019    3.5168    4.9837    7.0290    9.7844    13.6870    18.5990    24.2034
    1.1787    1.6232    2.2542    3.1578    4.4218    6.3096    8.8949    12.4209    16.9173    22.1389
    0.9879    1.3774    1.9128    2.6780    3.7750    5.3895    7.5992    10.6538    14.5778    19.0252
    0.7652    1.0602    1.4741    2.0768    2.9331    4.1695    5.9146    8.3144    11.4569    15.0440
    0.5158    0.7082    0.9910    1.4071    1.9908    2.8300    4.0271    5.7008    7.8525    10.4241
    0.2798    0.3887    0.5428    0.7661    1.0950    1.5544    2.2266    3.1685    4.3738    5.7960
    0.1100    0.1528    0.2146    0.3016    0.4283    0.6178    0.8848    1.2602    1.7554    2.3282
    0.0258    0.0361    0.0506    0.0719    0.1033    0.1485    0.2124    0.3023    0.4211    0.5623

```

0.0028	0.0039	0.0056	0.0079	0.0113	0.0163	0.0234	0.0333	0.0463	0.0616
0.0001	0.0001	0.0002	0.0003	0.0004	0.0006	0.0008	0.0011	0.0016	0.0021

gridRprobe(1:20,11:20) x10⁵ =

33.7326	38.6373	40.5204	39.3855	35.3638	29.8165	23.8897	18.9350	13.9330	11.0341
33.7446	38.7735	40.6830	39.2602	35.0910	29.8531	23.9767	18.4762	14.2771	11.0044
33.7279	38.3731	40.3960	39.3930	35.4466	30.1286	24.0857	18.8341	14.7092	10.9173
33.8172	38.6260	40.4958	39.4681	35.4686	29.4807	24.0782	18.6430	14.3358	10.7975
33.8261	38.5704	40.2056	39.2048	35.1713	29.6314	24.0409	18.3903	13.9332	10.2679
33.5670	38.2684	40.3266	39.0483	34.9500	29.1860	23.7121	18.3996	14.1294	10.9318
33.5697	37.9888	39.8441	38.7995	34.7685	29.1842	23.2917	18.1802	13.8229	10.0878
33.2904	37.7294	39.5146	38.4346	34.0965	28.7035	22.7764	17.6805	13.3975	9.8870
32.5986	36.9280	38.7559	37.2295	33.3040	28.2670	22.1673	16.9430	12.9890	9.5243
31.5024	35.9831	37.4829	36.0936	32.0139	26.6947	21.2088	15.7638	11.5672	8.3414
29.7338	34.1152	35.4249	33.7830	29.8710	24.6203	19.0033	14.0652	9.9464	6.7420
27.2212	31.0675	32.1297	30.4186	26.6517	21.4290	16.3495	11.7483	7.9667	5.2441
23.4971	26.7384	27.5217	26.0341	22.2518	17.4489	12.8337	8.8970	5.6972	3.5409
18.6742	21.1525	21.5535	20.0770	16.8265	12.7515	9.0116	5.7994	3.5252	2.0293
12.8707	14.5297	14.7284	13.3643	10.8300	7.9609	5.2498	3.1506	1.7593	0.8784
7.2001	8.0827	8.0969	7.2077	5.6322	3.9153	2.4021	1.3365	0.6453	0.2827
2.8900	3.2467	3.2200	2.7954	2.1046	1.3713	0.7773	0.3788	0.1653	0.0629
0.7013	0.7842	0.7683	0.6529	0.4738	0.2922	0.1527	0.0663	0.0242	0.0075
0.0767	0.0868	0.0847	0.0711	0.0501	0.0292	0.0140	0.0054	0.0016	0.0004
0.0026	0.0029	0.0029	0.0024	0.0017	0.0009	0.0004	0.0001	0.0000	0.0000

Non-contact probe getRdprobe()

The subroutine getRdprobe() calculates the total diffuse R_d then the factor f_{esc} for a particular fiber spot size (radius $a = h \sin(q)$) as the probe is held at a height (h) above the tissue. See Eq. 1 in the manuscript. The analysis grids gridRd and gridfesc are listed below for the case of a half-angle of light delivery $q = 24.8^\circ$ and a height $h = 1$ cm. The 2D interpolation yields values for R_d and f_{esc} , and the product $R_d f_{esc}$ is the probe response to be used in least-squares fitting of the data. The effect of f_{coll} is here ignored since it becomes incorporated in the scaling factor K during the least-squares fitting. The least-squares fitting is a standard routine and is not included in this Supplement. The subroutine is listed:

```
function Rdprobe = getRdprobe(mua,musp,LMSPL,LMA,gridRd,gridfesc)
lmua = log10(mua);
lmusp = log10(musp);
Rd = griddata(LMSPL,LMA,gridRd,lmusp,lmua);
fesc = griddata(LMSPL,LMA,gridfesc,lmusp,lmua);
Rdprobe = Rd.*fesc;
```

which uses the following array gridRd() that holds the values for $R_d(m_a, m_s')$ and the array gridfesc() that holds the values of $f_{esc}(m_a, m_s')$:

gridRd(1:20,1:10) =									
0.8294	0.8398	0.8761	0.8793	0.8792	0.9043	0.9010	0.9206	0.8985	0.9318
0.7857	0.8141	0.8309	0.8448	0.8626	0.8836	0.8830	0.8963	0.9111	0.9190
0.7370	0.7577	0.7843	0.8105	0.8231	0.8413	0.8639	0.8754	0.9007	0.9085
0.6671	0.7043	0.7324	0.7624	0.7856	0.8119	0.8354	0.8498	0.8637	0.8713
0.5949	0.6335	0.6668	0.7010	0.7292	0.7556	0.7850	0.8119	0.8208	0.8496
0.5009	0.5494	0.5884	0.6260	0.6687	0.6977	0.7295	0.7545	0.7815	0.8102
0.4080	0.4529	0.5021	0.5475	0.5875	0.6286	0.6663	0.7057	0.7300	0.7555
0.3098	0.3558	0.4038	0.4529	0.5009	0.5440	0.5871	0.6284	0.6598	0.7040

0.2202	0.2637	0.3112	0.3603	0.4018	0.4577	0.5033	0.5495	0.5759	0.6171
0.1431	0.1802	0.2197	0.2591	0.3104	0.3533	0.3978	0.4541	0.5018	0.5452
0.0849	0.1113	0.1427	0.1780	0.2199	0.2636	0.3088	0.3567	0.4041	0.4457
0.0452	0.0621	0.0847	0.1104	0.1421	0.1772	0.2177	0.2597	0.3096	0.3539
0.0220	0.0319	0.0448	0.0618	0.0845	0.1105	0.1424	0.1782	0.2148	0.2614
0.0103	0.0152	0.0219	0.0314	0.0448	0.0616	0.0828	0.1098	0.1407	0.1769
0.0050	0.0072	0.0103	0.0151	0.0218	0.0313	0.0442	0.0614	0.0831	0.1107
0.0025	0.0035	0.0049	0.0071	0.0102	0.0151	0.0216	0.0311	0.0439	0.0610
0.0013	0.0018	0.0025	0.0035	0.0049	0.0071	0.0103	0.0148	0.0216	0.0312
0.0007	0.0009	0.0013	0.0017	0.0025	0.0035	0.0049	0.0070	0.0102	0.0149
0.0004	0.0005	0.0007	0.0009	0.0013	0.0018	0.0024	0.0034	0.0049	0.0070
0.0002	0.0003	0.0004	0.0005	0.0007	0.0009	0.0013	0.0018	0.0024	0.0034
gridfesc(1:20,1;20) =	0.9286	0.9362	0.9393	0.9525	0.9561	0.9653	0.9529	0.9603	
0.9193	0.9209	0.9300	0.9372	0.9378	0.9442	0.9446	0.9588	0.9555	0.9607
0.8980	0.8973	0.9139	0.9163	0.9244	0.9290	0.9396	0.9424	0.9433	0.9522
0.8649	0.8759	0.8901	0.9037	0.9071	0.9180	0.9232	0.9291	0.9428	0.9424
0.8257	0.8503	0.8564	0.8906	0.8974	0.9018	0.9125	0.9085	0.9084	0.9443
0.7845	0.8081	0.8298	0.8461	0.8630	0.8862	0.8933	0.8984	0.9128	0.9283
0.7329	0.7609	0.7883	0.8122	0.8339	0.8478	0.8634	0.8804	0.8863	0.9010
0.6647	0.7042	0.7206	0.7654	0.7865	0.8078	0.8581	0.8404	0.8587	0.9047
0.5872	0.6245	0.6729	0.6950	0.7470	0.7448	0.8042	0.8177	0.8266	0.8643
0.5019	0.5332	0.5794	0.6131	0.6616	0.6776	0.7444	0.7514	0.7801	0.8170
0.4011	0.4522	0.4966	0.5429	0.5771	0.6179	0.6668	0.6886	0.7393	0.7683
0.3058	0.3526	0.3973	0.4486	0.4938	0.5388	0.5786	0.6160	0.6535	0.6853
0.2175	0.2611	0.3059	0.3518	0.4006	0.4441	0.4962	0.5391	0.5852	0.6207
0.1401	0.1762	0.2180	0.2582	0.3049	0.3527	0.4041	0.4507	0.4970	0.5412
0.0820	0.1092	0.1401	0.1743	0.2161	0.2575	0.3000	0.3484	0.3922	0.4448
0.0443	0.0604	0.0818	0.1084	0.1390	0.1747	0.2146	0.2560	0.3026	0.3499
0.0214	0.0306	0.0436	0.0602	0.0817	0.1071	0.1373	0.1730	0.2139	0.2576
0.0101	0.0147	0.0214	0.0306	0.0435	0.0599	0.0814	0.1075	0.1386	0.1723
0.0048	0.0070	0.0101	0.0146	0.0210	0.0304	0.0427	0.0590	0.0814	0.1068

gridfesc(1:20,1;10) =

0.0229	0.0377	0.0388	0.0573	0.0957	0.1135	0.1228	0.2466	0.3059	0.4797
0.0305	0.0353	0.0466	0.0682	0.0909	0.1306	0.1547	0.2378	0.3042	0.3928
0.0289	0.0335	0.0535	0.0693	0.0949	0.1353	0.1824	0.2387	0.2909	0.3931
0.0300	0.0399	0.0523	0.0685	0.1005	0.1380	0.1715	0.2593	0.3253	0.4206
0.0345	0.0469	0.0639	0.0752	0.1128	0.1562	0.1907	0.2545	0.3065	0.3983
0.0388	0.0537	0.0637	0.0873	0.1167	0.1538	0.2076	0.2560	0.3395	0.4209
0.0492	0.0605	0.0768	0.1014	0.1250	0.1771	0.2192	0.2928	0.3626	0.4562
0.0611	0.0749	0.0896	0.1182	0.1551	0.1917	0.2467	0.3172	0.3904	0.4776
0.0797	0.0956	0.1123	0.1397	0.1771	0.2264	0.2710	0.3530	0.4176	0.4931
0.1163	0.1297	0.1490	0.1693	0.2188	0.2564	0.3164	0.4000	0.4670	0.5526
0.1717	0.1850	0.1981	0.2269	0.2695	0.3139	0.3786	0.4513	0.5228	0.5939
0.2684	0.2729	0.2851	0.3052	0.3387	0.3881	0.4440	0.5096	0.5899	0.6540

0.4183	0.4065	0.4119	0.4167	0.4486	0.4903	0.5394	0.5972	0.6535	0.7148
0.6071	0.5913	0.5766	0.5753	0.5939	0.6117	0.6460	0.6905	0.7368	0.7865
0.7987	0.7807	0.7637	0.7517	0.7474	0.7504	0.7695	0.7909	0.8230	0.8534
0.9235	0.9147	0.9007	0.8903	0.8813	0.8813	0.8817	0.8872	0.8975	0.9131
0.9802	0.9792	0.9729	0.9702	0.9650	0.9615	0.9573	0.9555	0.9578	0.9610
1.0004	1.0003	0.9987	0.9978	0.9966	0.9950	0.9932	0.9916	0.9909	0.9906
1.0051	1.0052	1.0050	1.0047	1.0045	1.0045	1.0045	1.0037	1.0037	1.0030
1.0060	1.0060	1.0062	1.0059	1.0059	1.0062	1.0058	1.0058	1.0058	1.0059

gridfesc(1:20,11;20) =

0.4893	0.5511	0.6189	0.7029	0.7361	0.7549	0.8732	0.9131	0.9034	0.9693
0.4878	0.5581	0.6222	0.6920	0.7397	0.8010	0.8598	0.9125	0.9298	0.9452
0.4820	0.5510	0.6328	0.7011	0.7616	0.7964	0.8601	0.9212	0.9259	0.9553
0.4817	0.5652	0.6378	0.7041	0.7826	0.8254	0.8814	0.9213	0.9262	0.9642
0.4871	0.5790	0.6624	0.7181	0.7835	0.8317	0.8891	0.9100	0.9464	0.9650
0.5042	0.6007	0.6766	0.7523	0.7816	0.8677	0.8689	0.9379	0.9556	0.9363
0.5379	0.6070	0.6879	0.7597	0.8172	0.8810	0.8853	0.9143	0.9515	0.9549
0.5608	0.6357	0.7237	0.7846	0.8320	0.8765	0.9179	0.9302	0.9675	0.9798
0.6059	0.6725	0.7421	0.7924	0.8690	0.9170	0.9316	0.9601	0.9657	0.9855
0.6185	0.7052	0.7763	0.8312	0.8860	0.9041	0.9272	0.9641	0.9764	0.9898
0.6701	0.7429	0.8040	0.8515	0.8992	0.9265	0.9509	0.9783	0.9777	0.9901
0.7195	0.7840	0.8443	0.8880	0.9189	0.9447	0.9651	0.9819	0.9947	0.9927
0.7717	0.8317	0.8740	0.9158	0.9396	0.9547	0.9735	0.9858	0.9940	0.9985
0.8275	0.8751	0.9069	0.9337	0.9564	0.9713	0.9858	0.9946	0.9998	0.9998
0.8844	0.9120	0.9388	0.9577	0.9709	0.9841	0.9940	0.9994	1.0033	1.0039
0.9317	0.9471	0.9630	0.9760	0.9866	0.9929	1.0002	1.0012	1.0034	1.0051
0.9678	0.9757	0.9832	0.9900	0.9959	0.9993	1.0029	1.0042	1.0046	1.0060
0.9920	0.9934	0.9964	0.9999	1.0017	1.0037	1.0047	1.0058	1.0057	1.0060
1.0031	1.0031	1.0038	1.0043	1.0049	1.0054	1.0058	1.0057	1.0063	1.0061
1.0058	1.0056	1.0056	1.0059	1.0061	1.0058	1.0063	1.0061	1.0063	1.0063